Applied Ocean Research 104 (2020) 102358

Contents lists available at ScienceDirect

Applied Ocean Research

journal homepage: www.elsevier.com/locate/apor

Design considerations of suction caisson foundations for offshore wind turbines in Southern China

Bo Liu[a], Youhu Zhang[b,*], Zhaorong Ma[a], Knut H. Andersen[c], Hans Petter Jostad[d], Donghua Liu[a], Aiguo Pei[a]

[a] Guangdong Electric Power Design Institute, Tianfeng Rd. 1, Science City, Huangpu District, Guangzhou, China
[b] Senior Engineer, Norwegian Geotechnical Institute, Sognsveien 72, 0855 Oslo, Norway
[c] Expert Adviser, Norwegian Geotechnical Institute, Sognsveien 72, 0855 Oslo, Norway
[d] Technical Director, Norwegian Geotechnical Institute, Sognsveien 72, 0855 Oslo, Norway

ARTICLE INFO

Keywords:
Offshore wind
Suction caisson foundation
Typhoon
Cyclic loading
Settlement
Installation

ABSTRACT

Suction caisson foundations are increasingly considered as a foundation solution for offshore wind farm development in China. This paper outlines the design considerations for developing a suction caisson supported jacket solution for an offshore wind farm in Southern China. Geotechnical analyses for four major aspects, ultimate limit state (ULS), serviceability limit state (SLS), fatigue limit state (FLS) and installation are discussed. The design challenges encountered in the project due to soft seabed and metocean characteristics (severe typhoon loading and dominant wind directions) and technical approaches adopted by the project are presented. Areas for further studies are identified and discussed. The purpose of this paper is to disseminate this knowledge and raise awareness of several important aspects.

1. Introduction

The offshore wind industry in China has seen a rapid development in recent years. The accumulated installed capacity reached 6.0 GW by the end of 2019, and an annual increase of 2–3 GW is projected in the years to come (NORWEP, 2019). The foundations supporting the offshore wind turbines in China take a variety of forms, including monopiles, tripod or tetrapod structures resting on piles or suction caissons, hybrid monobuckets (Ding et al., 2015), and high-rise pile cap foundations supported by pile groups (Qi et al., 2014). The diversity in the foundation forms is attributed to the geotechnical conditions which often feature normally consolidated soft clays of varying thickness near the surface, followed by more competent clays, silty clays, loose to dense sands or silty sands. In some areas, shallow bedrock combined with weak seabed sediments may lead to expensive foundation construction in rock.

Over the last few years, suction caisson foundations have been applied in the offshore wind industry as an alternative foundation solution to pile foundations. Caisson supported jacket structures are the most common, with several projects already completed, including Borkum Riffgrund Offshore Wind Farm 1&2 and Aberdeen Bay Offshore Wind Farm. Due to their relatively quick and quiet installation process and advantage in sites with shallow rock, suction caisson supported jackets are increasingly being considered as a foundation solution for several offshore wind developments in China. However, from a geotechnical point of view, the site conditions are complex and challenging and represent a clear contrast to the conditions in the North Sea where the existing caisson supported jackets are installed on dense sands or firm clays. The complex geotechnical conditions (soft and layered ground) and frequent typhoon events pose several design challenges that need to be carefully addressed.

This paper outlines the design considerations for developing a suction caisson supported jacket solution for an offshore wind farm in Southern China. Geotechnical design challenges encountered in the project and technical solutions adopted by the project are presented and areas for further studies are identified. The purpose of this paper is to disseminate this knowledge and raise awareness of several important aspects.

2. Overview of design aspects for suction caisson foundations supporting offshore wind turbine structures

As outlined by Sturm (2017), the geotechnical design of the caisson foundations for jackets supporting offshore wind turbines includes the

* Corresponding author.
E-mail addresses: liubo2@gedi.com.cn (B. Liu), youhu.zhang@ngi.no (Y. Zhang), mazhaorong@gedi.com.cn (Z. Ma), knut.h.andersen@ngi.no (K.H. Andersen), hans.petter.jostad@ngi.no (H.P. Jostad), liudonghua@gedi.com.cn (D. Liu), peiaiguo@gedi.com.cn (A. Pei).

https://doi.org/10.1016/j.apor.2020.102358
Received 14 April 2020; Received in revised form 20 August 2020; Accepted 7 September 2020

following four major aspects:

1) Ultimate Limit State (ULS). The ULS design verifies the foundation's capacity against the extreme loading event. It should demonstrate that the foundation has sufficient safety margin against failure for the possible extreme loading condition.
2) Serviceability Limit State (SLS): The SLS design verifies that the accumulated deformation of the foundation during the design life of the turbine, which is typically 25 years, falls within the specified limit.
3) Fatigue Limit State (FLS): The FLS design checks the fatigue life of the structural members of the wind turbine system. From a geotechnical perspective, this is mainly the foundation' stiffness and damping, which are input to the dynamic analyses of the turbine structure and have consequence on the fatigue load assessment.
4) Installation: The installation design evaluates the caisson foundation's penetration resistance, required and allowable suction pressure, installation risks and mitigation strategies.

In addition, Accidental Limit State (ALS) which is concerned with maximum load-carrying capacity for (rare) accidental loads such as boat impact and earthquake or post-accidental integrity for damaged structures (DNVGL, 2018) should also be considered if relevant. Furthermore, for the caisson foundation, the possibility of scour development and the need for scour protection design are critical questions and need to be addressed in the design. However, in this paper, the discussions have been limited to the four aspects outlined above. The specific design challenges posed by the geotechnical and metocean conditions have been summarised and how they were addressed in the project is presented.

3. Geotechnical conditions

3.1. Static shear strength profile

This section provides an overview of the geotechnical condition of the study area. Fig. 1 presents the measured tip resistance (q_c) and u_2 pore pressure of a representative cone penetration test (CPTU) performed within the footprint of the tripod structure at a turbine location. The seabed typically consists of a layer of normally consolidated soft clay. The thickness varies from a couple of meters to up to 10 m. It is a young marine, medium plastic clay. The top soft clay is underlain by layers of low to medium plasticity, over-consolidated, silty clay or clay. Medium dense to very dense, medium to coarse sand layers are sandwiched in between the fine-grained layers. The fines (i.e., clay and silt particles) content in the sand layers varies. These layers are formed in an alternating land and marine deposition environment. From about 40 m below the seafloor, there is strongly weathered rock. From a foundation design point of view, the soil conditions in the upper 40 m is of most relevance for the example location illustrated in Fig. 1.

Fig. 2 presents the undrained shear strength (s_u) profile and interpreted over-consolidation ratio (*OCR*) with depth. The undrained shear strength profile is determined by a comprehensive onshore laboratory testing programme consisting of anisotropically consolidated undrained triaxial compression and extension (CAUC/CAUE) tests, undrained direct simple shear (DSS) tests, as well as empirical correlation from CPTU measurements. A cone factor (N_{kt}), which converts the cone resistance to the undrained shear strength, of 20 was found to produce a reasonably good fit to the strengths measured by CAUC tests (denoted as s_{uC}). The CAUE and DSS tests suggest the following anisotropy ratios: $s_{uE}/s_{uC} = 0.5$, $s_{uD}/s_{uC} = 0.75$, where s_{uE} is the undrained triaxial extension strength and s_{uD} is the undrained direct simple shear strength.

A high estimate of the undrained triaxial compression strength (s_{uC}) is made based on correlation from CPTU with a N_{kt} factor of 15. Considerable scatter of response is noted for the layer from 4 to 9.5 m below seafloor. The fluctuation in the measured cone resistance is likely an indication of local variation of the sand inclusion. However, the CPTU measured quite high positive excess pore pressure (Fig. 1), suggesting an undrained penetration response. The interpretation of s_u from the cone resistance using the same cone factor as other layers is likely to over-estimate the undrained shear strength in this layer because the relative high q_c value is likely have been contributed by the sand mixture in the soil matrix.

As illustrated, low estimate (LE) and high estimate (HE) design

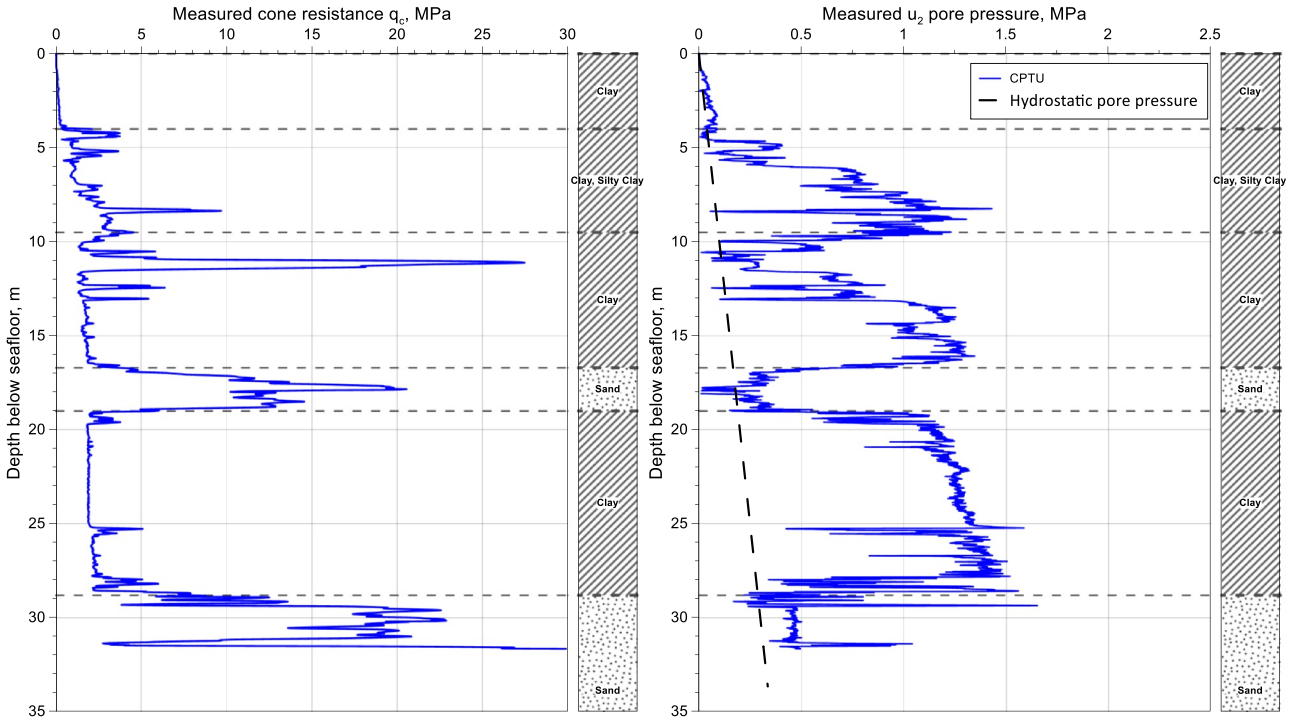

Fig. 1. CPTU cone resistance q_c and u_2 pore pressure at a representative turbine location.

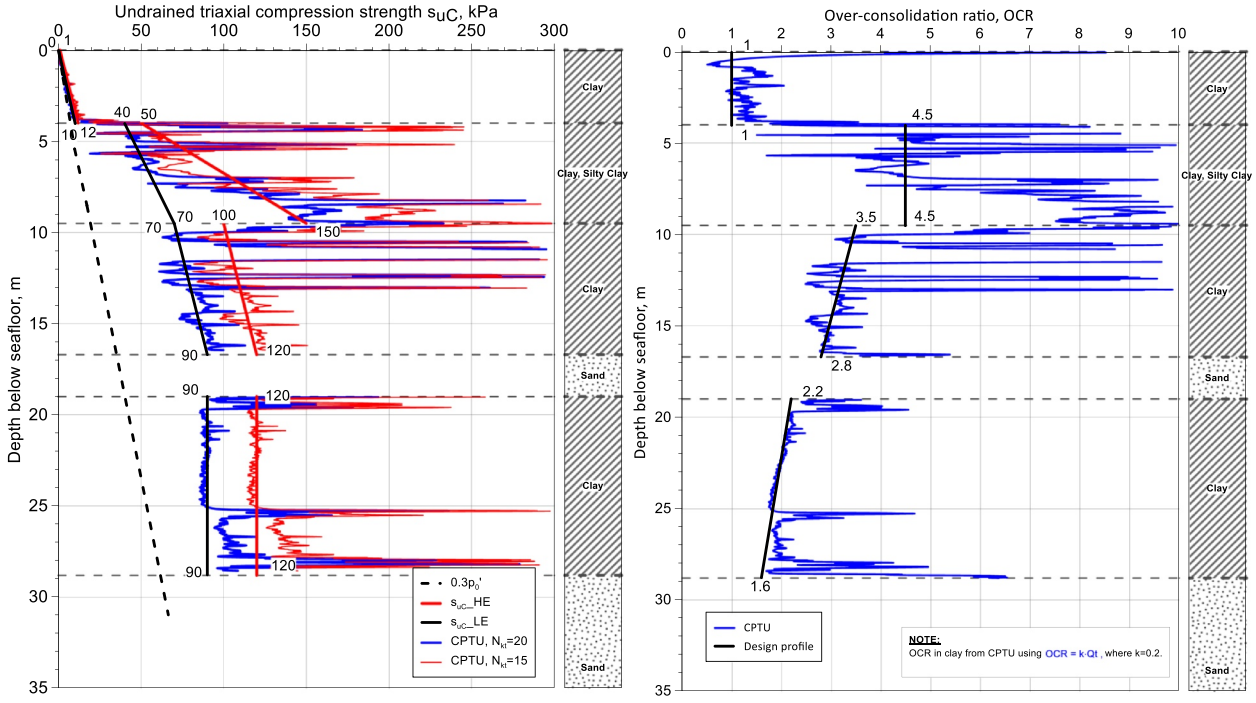

Fig. 2. Undrained shear strength (s_{uC}) and over-consolidation ratio (*OCR*) versus depth for a representative turbine location.

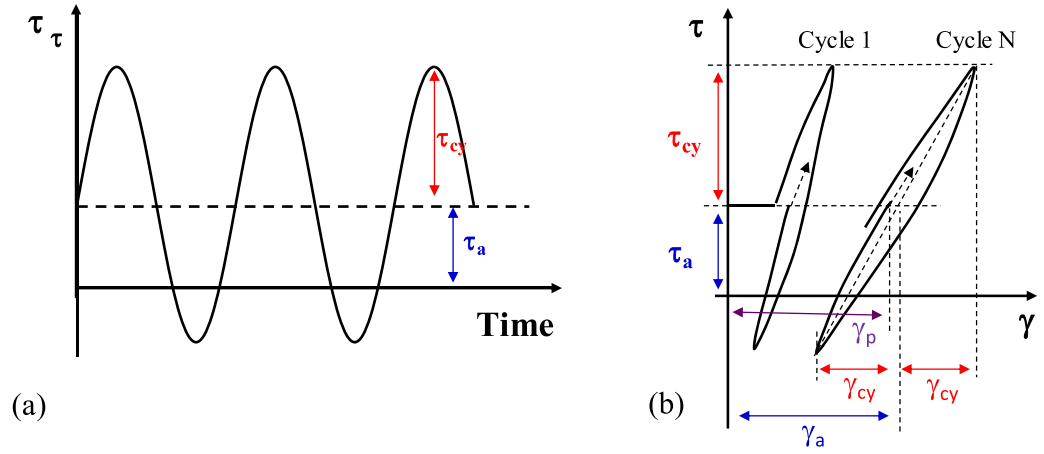

Fig. 3. Definition of: (a) average and cyclic shear stresses (τ_a, τ_{cy}); (b) average and cyclic shear strains (γ_a, γ_{cy}).

profiles for $s_{uC,}$ denoted s_{uC_LE} and s_{uC_HE} respectively in the figure, are proposed based on the CPTU correlation with $N_{kt}=20$ and 15 respectively. The labels next to the design lines indicate the s_{uC} values. For purpose of comparison, an empirical normally consolidation strength line, assuming $s_{uC} = 0.3p_{0'}$is also included, where $p_{0'}$is the in-situ vertical effective stress. The comparison clearly indicates over-consolidated state for the soil 4 m beneath the seafloor.

The pre-consolidation pressure p_c' and the over-consolidation ratio (*OCR*) are estimated from the CPTU measurement by the following equations according to Lunne et al. (1997):

$$p_c^{'} = k(q_t - \sigma_{v0}) \quad (1)$$

$$Q_t = \frac{(q_t - \sigma_{v0})}{\sigma_{v0}} \quad (2)$$

$$OCR = kQ_t \quad (3)$$

where

q_t is the total cone resistance

k is an empirical factor, which typically has a range from 0.2 to 0.5. Hereby $k = 0.2$ is used, which generates a reasonable agreement with the p_c' value measured from oedometer tests.

As illustrated in Fig. 2, the CPTU suggests that the top soft clay layer is normally consolidated while the soil layers below are over-consolidated. The over-consolidation ratio reduces gradually with the depth. A design *OCR* profile is proposed and illustrated in Fig. 2. The labels next to the design profile indicate the *OCR* values.

3.2. Cyclic properties

Wind turbine foundations are subjected to cyclic loading at almost all time due to various sources of vibrations (wind, wave and turbine rotations). However, the largest cyclic effect is expected during the extreme weather conditions. At the example turbine location, the clay layer from 9.5 m to 29 m belongs to the same geological unit and has a similar plasticity (with $I_p=25$), and a gradual reduction in *OCR*. For this reason, a batch of 10 cyclic DSS tests were performed between the depth interval from 10.82 m to 11.32 m to investigate the cyclic stress-

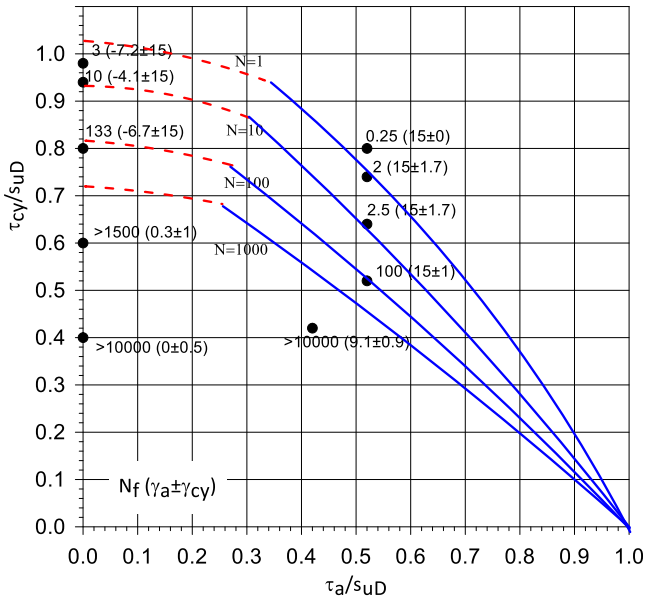

Fig. 4. DSS failure contours of the clay unit below 9.5 m (the label next to each data point indicates the number of stress cycles that bring the sample to failure, N_f, and the combination of average (γ_a) and cyclic (γ_{cy}) shear strains).

strain properties of this soil unit. At this depth interval, the *OCR* is estimated to be 3.4. Despite the variation of *OCR* over the depth of this layer, its effect on the normalized cyclic soil response is neglected. For ease of understanding, Fig. 3 defines the average and cyclic shear stresses (τ_a and τ_{cy}) as well as the resulting average and cyclic shear strains (γ_a and γ_{cy}).

The cyclic DSS tests were performed mainly at two different normalised average shear stresses: $\tau_a/s_{uD} = 0$ and $\tau_a/s_{uD} = 0.52$. The ten tests explore a range of different combinations of average and cyclic shear stresses and are used to construct the failure interaction diagram illustrated in Fig. 4. The diagram describes the stress combinations that cause failure of the soil specimen under specified number of cycles (1, 10, 100 and 1000). It should be noted that failure is defined as when either the average shear strain (γ_a) or the cyclic shear strain (γ_{cy}) reaches 15% as per Andersen (2015). Fig. 4 presents the γ_{cy}-log(N) contour diagram which describes the development of cyclic shear strain (γ_{cy}) with number of cycles (N) under symmetric cyclic shearing. It is constructed from the results of the five symmetric (i.e., $\tau_a/s_{uD} = 0$) cyclic DSS tests. The γ_{cy}-log(N) contour diagram will be used to determine the equivalent number of cycles (N_{eq}) for a cyclic loading history using the strain accumulation procedure, which is explained in detail in Andersen (2015). Fig. 6 presents strain contour diagrams which describe the development of average and cyclic shear strains (γ_a, γ_{cy} respectively) as a function of average and cyclic components of shear stress at different number of cycles. These diagrams will be used to derive the stress-strain curves of the soil for a given N_{eq} value and stress path (i.e., cyclic to average shear stress ratio), as will be demonstrated later. Fig. 5

From 16.7 to 19.0 m below the seafloor there is a loose to medium dense silty coarse sand layer with a q_c resistance between 10 and 15 MPa. Using the correlation presented by Jamiolkowski et al. (2003) and correcting for fines content (i.e., silt and clay content, which is assumed to be 10%), the relative density of this layer is estimated to be 50%. This type of loose to medium dense silty sand is widely distributed offshore China. The strength of these silty sand layers under cyclic loading requires close attention. Fig. 7 shows an empirical correlation of the 10-cycle undrained shear strength of normally consolidated sand and silt measured in DSS tests with symmetric cyclic loading. As illustrated, in the low relative density region (less than 60%), the cyclic shear strength, defined as cyclic shear stress causing 15% cyclic shear strain after 10 cycles, can get extremely low. The normalised strength ratio (τ_f/σ_{ref}') can be as low as 0.15, where σ_{ref}' is a function of the vertical consolidation pressure (σ_{vc}'), as detailed in Fig. 7. The sand has an *OCR* of 2.5 (inferred from the *OCR* of the clay layer above the sand), however, and this will increase the cyclic shear strength by a factor of about 2. In design of the turbine foundation at this location, the cyclic shear strength of the sand layer is estimated from the illustrated empirical database. Due to the relatively thin thickness of this layer and it is being sandwiched by thick competent clay layers above and below, the impact of this weak layer is relatively small for the dominantly vertical loading under the ULS condition. However, had this layer been thicker and located at shallower depth, this could have led to a very different result. Special attention should be paid to such loosely packed silty sand layers.

3.3. Challenges in characterisation of the site conditions in Southern China

Based on the experience from this project and other projects in the region, we observe several common challenges in terms of characterising the soil conditions:

1) Interpretation of CPTU results. There is still limited regional experience for interpretation of CPTU results for offshore wind development in Southern China. This introduces uncertainties when correlating the CPTU measurements to soil parameters. The seabed soil in Southern China is typically consisted layered soft clay, silty sand and silty clay, and interpretation of silty material is known to be challenging. Efforts to compare CPTU results and companion advanced lab tests on high quality soil samples are urgently needed to verify existing correlations established from other regions or to develop new regional correlations.
2) Cyclic soil properties, particularly for the wide-spread silty sands. Similar to CPTU interpretation, there exists relatively little experience on the cyclic properties of soils from offshore China. In particular, the wide spread of loosely packed silty sand layers poses a significant design challenge which requires special attention.
3) Engineering geology. Geology tells the story of the genesis of the soils and its history. It fundamentally controls the engineering properties of the soil. Geotechnical investigation of the ground condition should be performed together with an engineering geology understanding. This understanding should support and verify the geotechnical interpretations. For example, if a soil layer is interpreted to be heavily over-consolidated by geotechnical investigation, the cause of this *OCR* should be explained by engineering geology. Due to the complex geological settings in many offshore wind development sites in Southern China, this aspect should be emphasized.

4. Ultimate limit state

4.1. Typhoon loading

The project area is subjected to frequent tropical cyclones, i.e., typhoons. In addition to extreme wind speed, the typhoons cause severe wave conditions. The wind turbines in this project are designed to withstand a 50-year return typhoon. At the hub level (~110 m above sea level), the speed of 3 s extreme gust is 71.8 m/s (258 km/h) and the 10 min mean wind speed is 55.2 m/s (199 km/h). The significant wave height during the peak stage of the typhoon is 10.12 m, with a period of 17.1 s. The maximum wave height (H_{max}) is 18.43 m.

4.2. Cyclic effects and uls load time histories

To verify the foundation's capacity against the extreme loading during the 50-year return typhoon event, the effect of cyclic loading must be accounted for. Prior to the arrival of the extreme wind speed

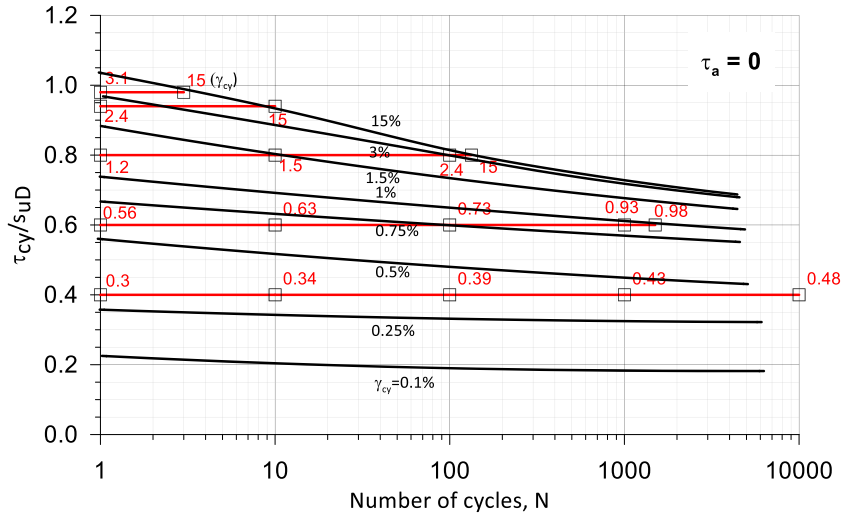

Fig. 5. Cyclic shear strain with no. of cycles for symmetric cyclic DSS tests.

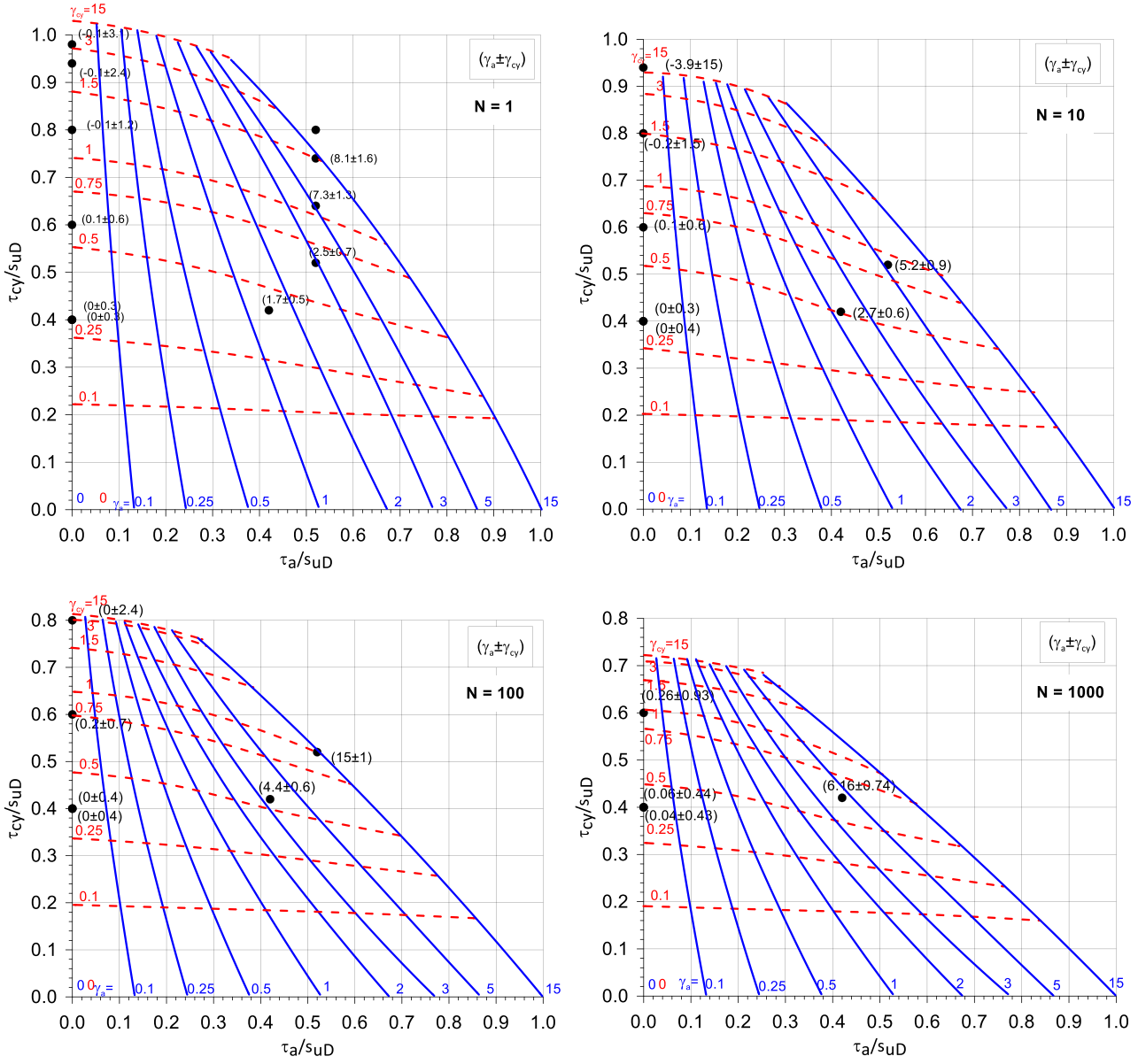

Fig. 6. Cyclic and average shear strain contour diagrams for DSS condition.

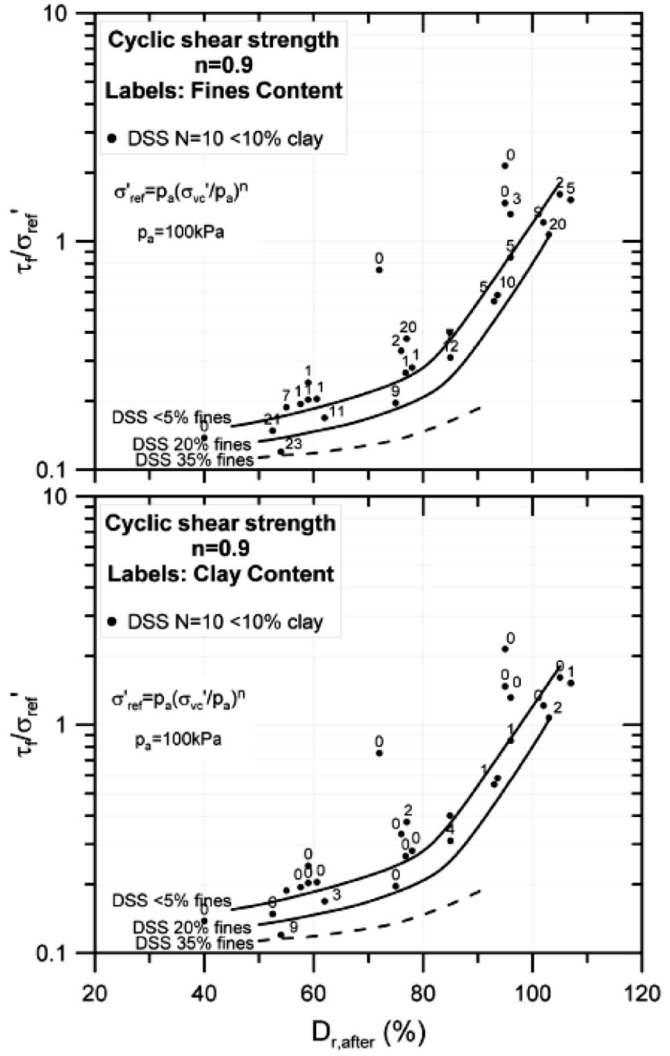

Fig. 7. Cyclic shear strength with 10 cycles of symmetric cyclic loading in DSS for normally consolidated sand and silt (from Andersen, 2015).

Table 1
Make-up of the 50-year return typhoon.

Stage	10 min mean wind speed at hub level, m/s	H_s, m	T_p, s	Duration, h
1	30	4.2	10.5	10
2	40	5.59	12.7	6
3	55.2	10.12	17.1	2

and wave, there are smaller cyclic loads which cause an accumulation of pore pressure in the soil. This reduces the strength and stiffness of the soil before the maximum load arrives. For this purpose, the complete time history of the cyclic loads on the caisson foundation during the 50-year return typhoon is ideally required. However, there is no standardised 50-year return typhoon event specified in the code for geotechnical design. Based on monitored data of past typhoon events, an 18-hour typhoon event is proposed in the project, as detailed in Table 1. The typhoon is assumed to consists of three idealised stages, with the 10-mins mean wind speed and significant wave height increasing with time. The total duration of the typhoon is assumed to be 18 h, and the peak stage is assumed to last for 2 h. For each stage of the typhoon, six time domain simulations are performed in order to capture the randomness of the stochastic process, with the 10-min mean wind speed, significant wave height (H_s) and wave period (T_p) as input parameters. In each of the 10-min time domain simulations for the peak stage, a constrained wave corresponding to the maximum wave (H_{max}) is inserted. Such time domain analyses are performed for orientations that produce either the maximum compression load or the maximum tension load on one of the three caisson foundations.

Fig. 8 presents two examples of 10-min time histories during the stage 3 (peak stage) for the ULS typhoons causing maximum compression loading and maximum tension loading respectively. The wind and wave directions are assumed to coincide. The blades are free to rotate, and the yaw control system is assumed to malfunction due to loss of power. Thus, the blades do not face the wind perpendicularly, as illustrated in Fig. 9. Fig. 8(a) illustrates that the inserted maximum wave (at about 100 s) generates a considerably larger compression load compared to the rest of the time history. The two unloaded foundations (Bucket 1 and Bucket 2) remain in compression for the most part of the time, except when the maximum wave hits the turbine. Fig. 8(b) illustrates that for the maximum tension orientation, the long term average load stays almost neutral. Similar to the compression loading, the inserted maximum wave at 100 s generates a tension loading that is considerably higher than the rest. However, in this 10-min simulation, another maximum wave is realised, generating a slightly higher tension loading.

For each stage of the typhoon, the six 10-min time histories are counted using the rain-flow method. They are then sorted into packages. The total number of cycles during each stage of the typhoon is then derived by multiplying the number of hours with the cycles counted for the six realisations, which correspond to 1 hour. Note that although maximum wave (H_{max}) is constrained to occur during each of the six 10-min time domain simulations for the peak stage, only one load cycle generated by the constrained maximum wave is considered during the entire typhoon.

Once the sorted load packages are determined, the equivalent number of cycles of the largest cyclic load (N_{eq}) that will correspond to the entire typhoon load history is calculated using the strain accumulation procedure for clay and the pore pressure accumulation procedure for sand. The procedures are described in detail in Andersen (2015) and are therefore not repeated here. The cyclic undrained shear strength of the soil is then extracted from the contour diagrams, based on the N_{eq} and the ratio of cyclic component to the average component of the largest loading cycle. This is demonstrated in Fig. 10, which illustrates an assumed cyclic to average stress ratio of 0.65. The stress path (black solid line in Fig. 10a) intersects with the average and cyclic strain contour lines. The intersection points define the average shear stress-average shear strain (τ_a-γ_a) and cyclic shear stress-cyclic shear strain (τ_{cy}-γ_{cy}) curves. The summation of the average and cyclic shear stress-shear strain curves gives the total shear stress and total shear strain curve. The total stress-strain curve is de-normalised by the reference static strength and used as input for ULS bearing capacity analysis.

Sturm (2017) also discussed another ULS loading scenario where one of the caisson foundations is under sustaining net uplift loading when the turbine is in a normal power generation state under relatively high wind speed. This has been checked, and it was found not relevant for this project.

5. Serviceability limit state

For the normal functioning of the wind turbine, the displacements of the jacket structure, particularly the tilt, must be controlled to be within a certain limit. The allowable limit is a decision that must be taken by the operator of the wind farm and the turbine manufacturer as it is fundamentally related to what level of tilt that is acceptable for the turbine. The offshore wind industry seems to generally adopt a 0.5° criterion for bottom-fixed turbines, half of which is normally assigned to the installation tolerance, leaving only 0.25° for accumulated tilt during the operational life of the turbine. The 0.5° originates from the DNVGL standard (DNVGL 2018) despite that the number is not really meant as a prescription.

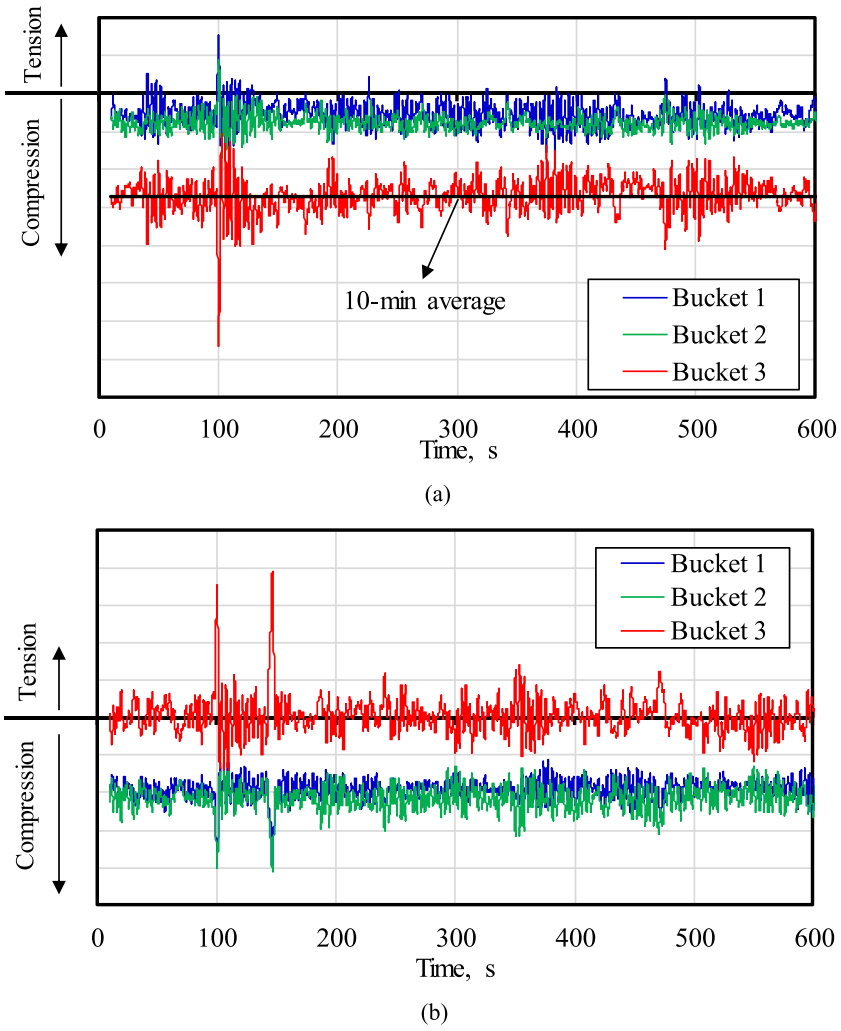

Fig. 8. Example of 10-min time load histories: (a) for maximum compression loading; (b) for maximum tension loading.

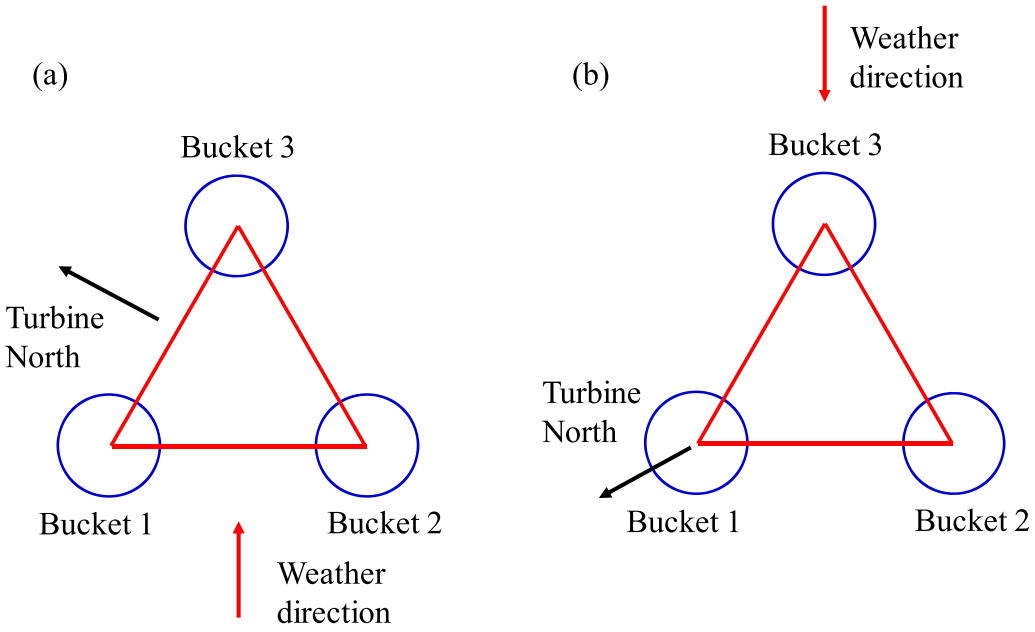

Fig. 9. Weather direction with respect to turbine orientation: (a) maximum compression; (b) maximum tension.

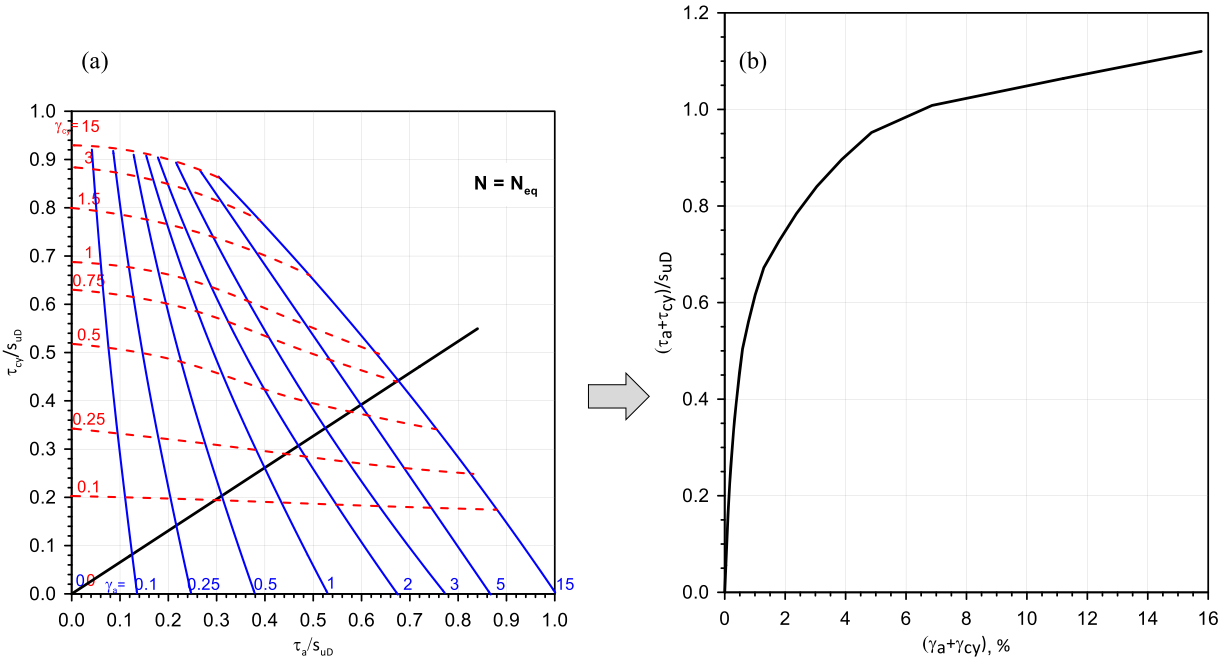

Fig. 10. Extraction of stress-strain curve from the strain contour diagram based on N_{eq} and stress path: (a) τ_a-γ_a and τ_{cy}-γ_{cy} stress-strain curves; (b) total stress-strain curve.

For a three-legged jacket supporting structure, the accumulated tilt of the wind turbine is most likely caused by the differential vertical deformation amongst the three legs. Considering the stiff connection between the leg and the bucket, local rotation of the bucket foundation is unlikely. The vertical settlement of the bucket foundations can be caused by the following mechanisms:

1) Plastic deformation due to repeated loading (i.e., permanent shear strain due to cyclic shearing at soil element level)
2) Dissipation of pore pressure generated by the average vertical loading under normal power production.

In this section, the design consideration and challenges associated with the above-mentioned aspects are discussed.

5.1. Accumulated displacement due to cyclic loading

Soil accumulates shear strain due to repeated cyclic shearing. On a macro scale, this is manifested by accumulated foundation displacement. During its service life, the turbine will experience multiple typhoons. How to assess the accumulated foundation displacement due to all those typhoons is not an easy question.

5.1.1. Accumulated displacement due to 50-year return typhoon

The 50-year return typhoon is assumed to occur once during the design life of the wind turbine. Fig. 11 presents a schematic illustration of the calculation philosophy. Fig. 11a illustrates the development of average (γ_a), cyclic (γ_{cy}) and permanent (γ_p) shear strain with cyclic loading on a soil element level while Fig. 11b illustrates the development of foundation displacement. Here in this project, the accumulated foundation displacement is approximately taken to be the average displacement (as illustrated in Fig. 11b) at the end of the cyclic loading minus the rebound when the average load component is unloaded. The rebound is assumed to be elastic and controlled by initial stiffness of the soil. In principle it is more correct to calculate the accumulated displacement from the permanent displacement (as illustrated in Fig. 11b). However, as strain contour diagrams are typically expressed in terms of γ_a and γ_{cy} instead of γ_p and γ_{cy}, it is easier to calculate the average displacement using the γ_a - τ_a response extracted from the strain contours, as will be explained below. The approximation made here will lead to somewhat higher estimated accumulated foundation displacement.

Similar to the ULS bearing capacity analysis, the equivalent number of cycles (N_{eq}) and the cyclic to average loading ratio is used to extract the stress-strain response from the strain contour diagram. However, in order to calculate the average foundation displacement, only the average component of stress-strain response (τ_a-γ_a) is used as input to FEA and the average foundation loading component is applied in FEA. The displacement calculated by FEA then corresponds to the average displacement. An unloading step using G_{max} soil parameters then calculates the elastic rebound when the average component is unloaded. It should be noted that the load and material parameters are not factored in this calculation.

The above described procedure is repeated for both the compression leg and for the tension leg. The total difference in accumulated vertical displacement is then used to calculate the accumulated tilt due to the 50-year return typhoon event by taking consideration of the leg to leg spacing.

5.1.2. Accumulated displacement due to smaller typhoons

In addition to the 50-year return typhoon, the turbine will experience several smaller typhoons during its service life, for example 10-year return typhoons and 5-year return typhoons. Each of them might have more than one occurrence. In principal, the methodology applied for the 50-year typhoon can be applied to the smaller typhoons. However, the big question is how the displacements from the different events and multiple occurrences of the same event should be combined to give the total accumulated displacement.

There are several possible approaches:

1) Evaluate accumulated displacement of each loading event, multiply by the number of occurrences and sum up all events. For example, if the 10-year typhoon is estimated to occur 3 times during the service life of the turbine, the accumulated foundation displacement for a single 10-year typhoon is first calculated using the approach described above for 50-year return typhoon, then the accumulated

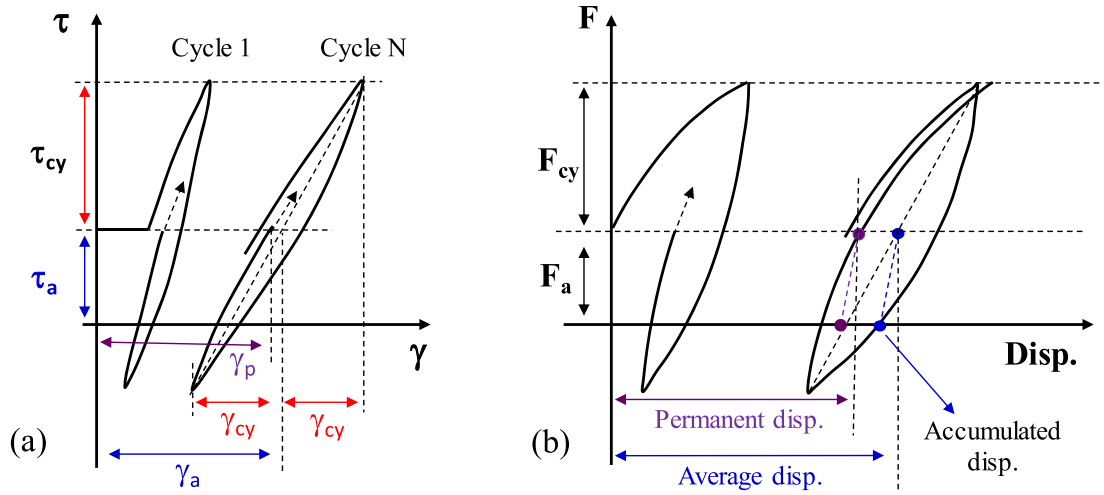

Fig. 11. Schematic illustration of calculation philosophy for accumulated foundation displacement due to cyclic loading: (a) response at soil element level; (b) response at foundation level.

displacement by all 10-year return typhoons will simply be 3 times. This will be summed up with accumulated displacements caused by other loading events (i.e., 50-year return typhoon etc.). This approach is considered to be too conservative as it is well established that soil strain development under cyclic shearing is not linear to the number of load cycles.

2) Lump all loading cycles from all occurrences of the same return period typhoon into one "super" typhoon, calculate its accumulated displacement and sum up with displacements caused by typhoons of other return periods. In this approach, the weakness of the approach discussed above is dealt with. However, it still assumes that the accumulated displacements due to smaller typhoons can be superimposed with those due to larger typhoons, which may over-estimate the total accumulated displacement.
3) Lump all loading cycles from all typhoons expected during the life time of the turbine into one "full-life" typhoon. In this approach, the loading cycles due to the smaller typhoons will most likely to be over-shadowed by cycles from larger typhoons and contribute little to the overall N_{eq} and therefore the accumulated displacement.

Based on the above discussions, we chose to adopt the second approach in this project. It was found that the accumulated displacement due to the 50-year return typhoon had the largest contribution to the accumulated tilt.

There are several fundamental assumptions that are made in the above assessment:

1) It is assumed that the most and the least loaded legs coincide in all typhoons so the accumulated displacements from different typhoons can be superimposed. This is clearly a major assumption and will lead to the worst scenario (i.e., largest accumulated tilt).
2) The effect of consolidation between typhoons are neglected. After a typhoon event, pore pressure generated by cyclic loading will dissipate during the calm period. This could lead to a "hardening" effect in soft soils and will reduce the soil's response when it is subjected to cyclic loading again. This effect is currently not considered.
3) The caisson foundations are subjected to a long-term average vertical load under normal operation. This will pass an increased vertical stress to the soil below the skirt tip, which will consolidate the soil and have a positive effect on the soil strength. However, the effect is dependant on the in-situ soil state (sand or clay, normally consolidated or over-consolidated etc.).

5.2. Consolidation settlement under long term operation

5.2.1. Wind direction and foundation loads for consolidation settlement calculation

In this project, there is a clear dominant wind direction. This is illustrated by Fig. 12 which shows the relation between the dominant wind direction with respect to the wind turbine layout. The wind from North-East direction is dominant. Under normal power production, it can be expected that the turbine will be subjected to a wind load coming from the NE direction for the most of its operational time. For the consolidation settlement calculation, it is therefore decided to use the foundation loads calculated for normal power production under the annual mean wind speed with the wind from the dominant direction. It can be expected that Bucket 1 and Bucket 3 will be subjected to higher vertical loads than Bucket 2. A load factor of 1.0 is used for settlement calculations.

5.2.2. Computation model

Fig. 13 presents the consolidation settlement calculation model. The external load (F), which includes the contribution of the self-weight of the bucket, is resisted by the internal and external skin frictions (F_{s_in} and F_{s_ex} respectively), skirt tip resistance F_t and the base plate bearing by the internal soil plug as illustrated by Fig. 13. It is assumed that the external skin friction is transmitted to far field, while the internal skin friction is transmitted to the soil plug and subsequently to the soil below the skirt tip. The load taken by the skirt tip (F_t) is also assumed to be transmitted uniformly to the soil below the tip level. In clay, F_t is

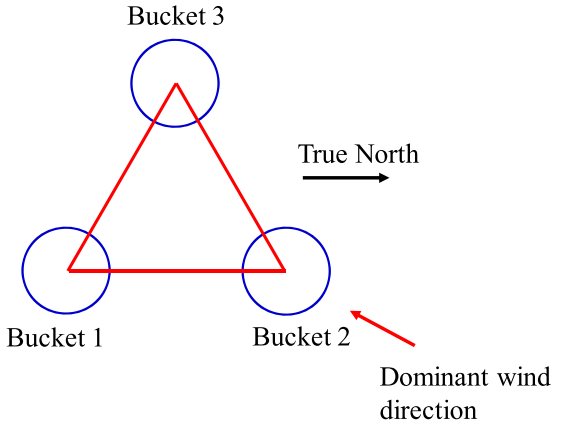

Fig. 12. Dominant wind direction with regard to the turbine layout.

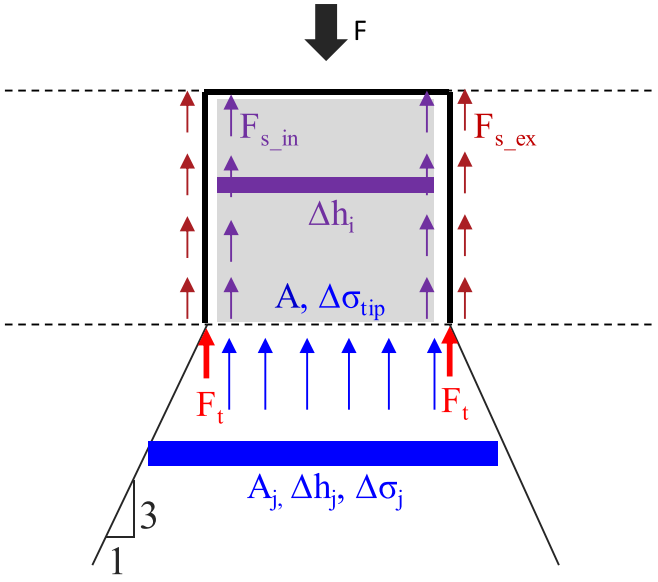

Fig. 13. Consolidation settlement calculation model.

small compared to the side frictions and can be practically ignored. It is however a very important component if the skirt tip sits in sandy soils. Below the skirt tip level, the additional stress resulting from the caisson foundation is assumed to reduce with depth due to a 3 (vertical) to 1 (horizontal) load spread.

To compute the settlement, the soil within the caisson foundation and below the skirt tip are divided into a series of horizontal slices. The additional stress ($\Delta\sigma$) is evaluated for each of the horizontal soil slices. The settlement on each slice is then calculated by considering its compressibility (i.e., constrained modulus) and its height (Δh). The total consolidation settlement is an integration of settlement from all soil slices. In Liu et al. (2020), methods to compute the internal, external skin frictions and tip resistance are presented. Equations to calculate the additional stresses for soil slices within the suction caisson and below the skirt tip are detailed. Liu et al. (2020) also discuss the selection of soil parameters for the settlement assessment. An example case is presented to demonstrate the application of the proposed model.

6. Fatigue limit state

From a geotechnical perspective, the fatigue limit state design is concerned with the foundation-soil interaction (stiffness and soil damping) which is incorporated into the structure fatigue stress assessment. Time domain structural simulations are commonly performed, with the foundation-soil interaction incorporated as non-linear/linear springs (for stiffness) and dashpots (soil damping). An alternative approach is to incorporate the foundation-soil interaction as macro models (for example Skau et al., 2018), which capture the multi-directional load interaction, stiffness reduction with load level and the soil damping in a constitutive framework. This study limits the discussion to the conventional approach, i.e., foundation springs. Soil damping is not discussed here.

The foundation springs have an impact on the structural fatigue assessment as they influence the natural frequency of the turbine system, which in turn influences how close the system's frequency is to the excitation frequencies (e.g. wind, wave, 1P and 3P). This section will discuss the different aspects that require special attention when calculating the FLS foundation stiffness.

6.1. Foundation loads for FLS stiffness calculation

Assuming that the majority of the structural fatigue damage is induced during the normal power generation, the fatigue stresses on the structural members can be assessed for conditions at a range of representative wind speeds. The accumulated fatigue damage can then be assessed by considering the proportions of the time during which the turbine is operating at different wind speeds, based on the wind speed statistics. For each wind speed, the foundation stiffness should be evaluated based on a priori assessed foundation load under that wind speed. An iterative process is therefore involved for conformity between the foundation loads and the foundation stiffness.

The foundation loads are cyclic in nature and contains an average component and a cyclic component, as illustrated in Fig. 14 as an idealised sinusoidal load series. During the structural vibration, the foundation stiffness felt by the structure is the cyclic stiffness, i.e., the peak to peak stiffness implied by the cyclic load-displacement loops instead of the total secant stiffness (dashed blue line in Fig. 14). Therefore, when computing the foundation stiffness for fatigue assessment, it is the cyclic component of the foundation loads that should be used.

6.2. Soil input parameters for FLS stiffness calculation

Under normal power production, the foundation loads are only a small proportion of the ULS load. In addition, the foundation is sized to give a safety factor (load factor * material factor) against the ULS load. It is assumed that the operational loads will not cause meaningful cyclic

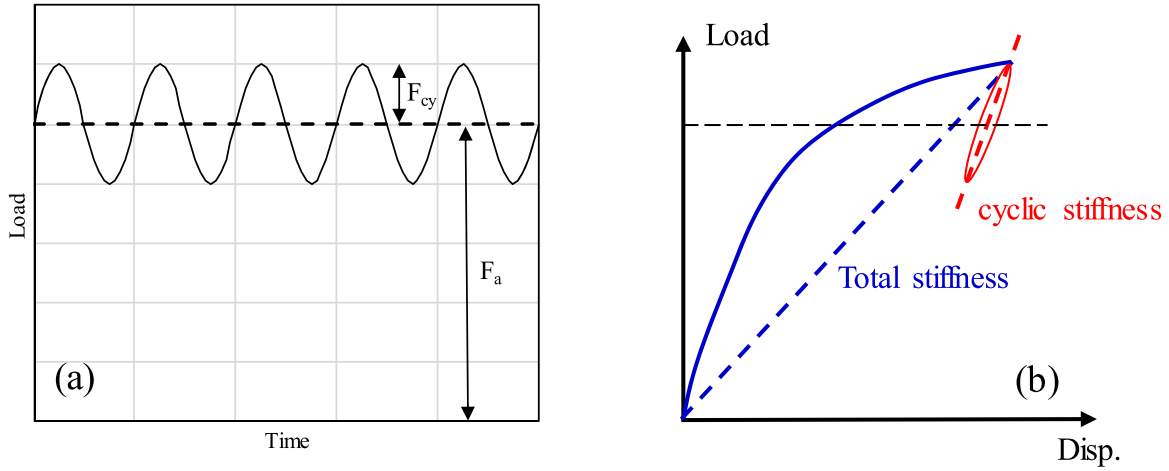

Fig. 14. (a) Illustration of the average load (F_a) and the cyclic load (F_{cy}) components of a load history, and (b) corresponding total secant stiffness and cyclic secant stiffness.

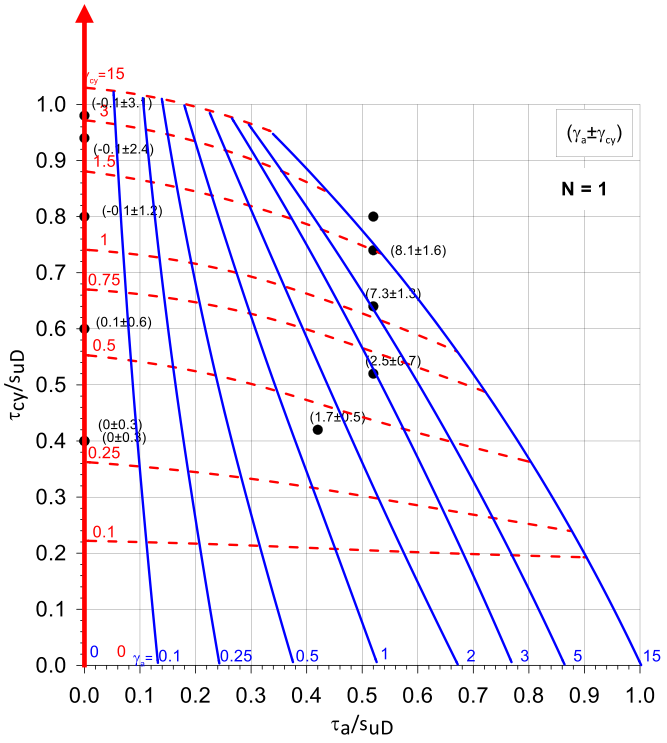

Fig. 15. Extract the cyclic stress-strain curve for FLS foundation stiffness calculation.

accumulation effect in the soil.

To compute the cyclic foundation stiffness, the cyclic stress-strain response of the soil is needed as input. This can be extracted from the cyclic strain contour diagrams for $N = 1$, as illustrated by Fig. 15. However, one thing requires particular attention is that the smallest cyclic contour line is 0.1%. There is no point in-between zero and 0.1% cyclic shear strain. Considering the very small load level analysed here, it is necessary to capture the nonlinearity of the soil response in this very small shear strain range. For this purpose, the stiffness reduction model proposed by Darendeli (2001) is used to curve-fit the soil response extracted from the strain contour diagrams. The Darendeli model describes the stiffness reduction using the following function:

$$\frac{G}{G_{max}} = \frac{1}{1 + \left(\frac{\gamma}{\gamma_r}\right)^a} \tag{4}$$

where

G is the cyclic shear modulus mobilised at a cyclic shear strain amplitude γ;

$G_{\max}$ is the initial stiffness of the soil;

γ_r is a curve fitting parameter, which physically means the cyclic shear strain amplitude at which the mobilised cyclic shear modulus is reduced to half of $G_{\max}$;

a is a curve fitting parameter, which regulates the curvature of the stiffness reduction curve.

The $G_{\max}$ of the soil is typically measured in a site investigation, either offshore by seismic CPT, or in the onshore laboratory, such as by resonant column or bender element tests. There are also empirical correlations for sand (e.g. Seed and Idriss, 1970; Hardin and Drnevich, 1972) and for clay (Andersen, 2015). Fig. 16 illustrates the curve-fitting of the Darendeli stiffness reduction model, which captures the stiffness reduction for cyclic shear strains less than 0.1%. Reflected on the cyclic stress-strain curve, a non-linear curve starting from $G_{\max}$ is used instead of a straight line between 0% and 0.1% cyclic shear strain.

6.3. Coupling between the horizontal and rotational degrees-of-freedom

When computing the foundation stiffness for caisson foundations, a common issue is the coupling between the horizontal and rotational degrees-of-freedom, i.e., a horizontal load will not only cause a horizontal displacement but also a rotation at the lid level, and vice versa. When expressing the foundation stiffness as springs, it is difficult to incorporate the coupling term of the stiffness matrix. To deal with this challenge, the method proposed by Hansteen (1984) and applied by Carswell et al. (2015) can be used. The method expresses the foundation stiffness at the so-called "de-coupling" point where the horizontal and moment degree-of-freedoms are de-coupled. In the structural analysis, a rigid beam can be used to connect the leg to the de-coupling point where the foundation springs are attached. It should be noted that due to the soil nonlinearity, the de-coupling point is not fixed in space but rather changes its position depending on the load level. It should therefore be established at the load level of interest. As illustrated in Fig. 17, in order to find the depth of the de-coupling point in the XZ plane, a numerical perturbation analysis is performed with a small increment in M_y while maintaining all other load components unchanged. Compared to the base case analysis, the small positive increment dM_y results in a positive rotation increment $d\theta_y$ and a positive horizontal displacement increment du_x. The depth of the de-coupling point L_{XZ} can be calculated:

$$L_{XZ} = \frac{du_x}{d\theta_y} \tag{5}$$

Positive sign of L_{XZ} means depth below the interface point which is at the centre of the bucket lid.

The horizontal foundation stiffness in X axis direction (K_x) and the rotational stiffness about Y axis ($K_{\theta y}$) at the de-coupling point is then:

$$K_x = \frac{F_{x\_dc}}{u_{x\_dc}} = \frac{F_x}{u_x - \theta_y L_{XZ}} \tag{6}$$

$$K_{\theta y} = \frac{M_{y\_dc}}{\theta_{y\_dc}} = \frac{M_y + F_x L_{XZ}}{\theta_y} \tag{7}$$

Similarly, in the YZ plane, it can be demonstrated that:

$$L_{YZ} = -\frac{du_y}{d\theta_x} \tag{8}$$

The negative sign is because that a positive increment in moment about the X axis will cause a positive increment in rotation about X axis, but a negative increment in horizontal displacement in Y axis. A positive sign of L_{YZ} represents a de-coupling point below the bucket lid.

The horizontal foundation stiffness in Y axis direction (K_y) and the rotational stiffness about X axis ($K_{\theta x}$) stiffness at the decoupling point is:

$$K_y = \frac{F_{y\_dc}}{u_{y\_dc}} = \frac{F_y}{u_y + \theta_x L_{YZ}} \tag{9}$$

$$K_{\theta x} = \frac{M_{x\_dc}}{\theta_{x\_dc}} = \frac{M_x - F_y L_{YZ}}{\theta_x} \tag{10}$$

Similar depths of the decoupling point are normally calculated in the XZ and YZ planes. An average value of the two can be used.

6.4. Flexibility of the foundation lid

In finite element calculations of caisson foundations, the caisson foundation is often treated as a rigid body. This is considered appropriate for the bearing capacity analyses. However, caution is needed when it comes to the FLS foundation stiffness, for which, the flexibility of the bucket itself might alter the overall soil-foundation interaction stiffness. This is identified by field measurements (Shonberg et al., 2017) and studied in detail by Skau et al. (2019) who concluded that the flexibility of the bucket lid has the largest impact on the system

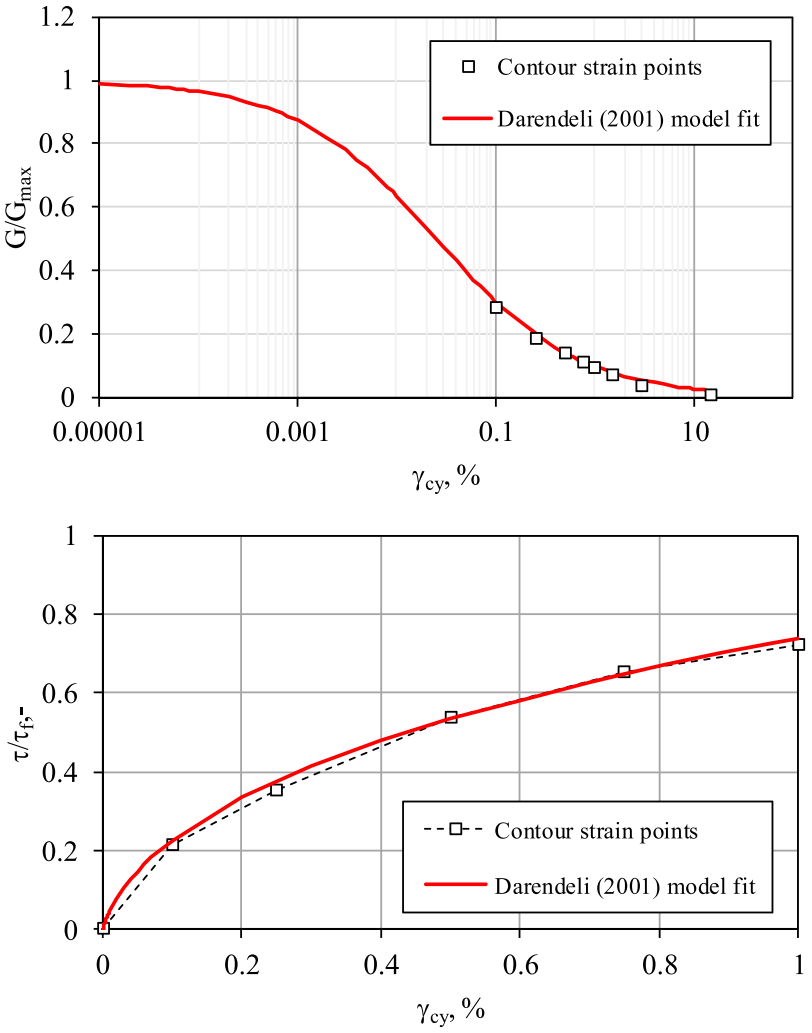

Fig. 16. Curve fitting of the stress-strain response at small strain levels.

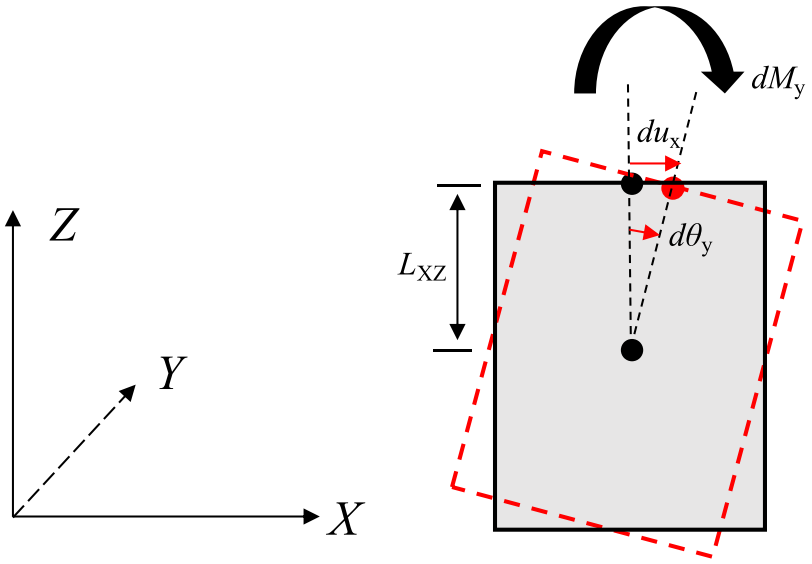

Fig. 17. Finding the de-coupling point through numerical perturbation analysis.

stiffness while the skirt has negligible impact.

7. Installation

The mechanism for suction caisson installation in clean sand or pure clay is well understood and design methods for calculating the installation resistance, required and allowed suction pressure, and plug uplift is well established (Housby and Byrne 2005; Andersen et al., 2008; Senders and Randolph 2009; DNVGL, 2017). However, when it comes to layered soils, particularly, in clay over sand soil profiles, installation design is not straightforward and there are still large uncertainties. In this project, the seabed typically consists of a layer of soft clay on the surface. Below this surface layer often lies sandy layers. This poses a challenge in case of those conditions.

The largest uncertainty for suction caisson installation in a clay over sand soil profile is whether seepage flow is developed in the sand. Without the seepage flow, large skirt tip resistance can be encountered (e.g. Andersen et al., 2008). The required suction pressure can be typically too high compared to what is allowable structurally (buckling) and what is feasible due to relatively shallow water depths for offshore wind turbines (i.e., cavitation limit). Senders et al. (2007) hypothesized a theory that in a clay over sand profile, once the applied suction overcomes the self-weight and the side friction on the internal soil plug, the suction pressure will be transferred to the clay-sand interface. This will cause a formation of seepage flow in the sand, which reduces the skirt tip resistance, but also causes a risk of large inside plug heave that can prevent full skirt penetration. Klinkvort et al. (2019) developed this theory further, and proposed methods to calculate the installation resistance in the underlying sand layer and the amount of plug uplift due to seepage through the sand but confined by the upper clay. However, this theory and calculation model is yet to be validated by experiments or field installations before the proposed methods can be confidently relied on.

Sparrevik and Strout (2015) suggest that "cycling", i.e., pressure reversal and even limited uplift movement during the caisson installation, can be a very useful method for reducing the installation resistance, although the mechanism behind this reduction is not fully understood.

8. Concluding remarks

This paper presents a methodology adopted for design of suction caisson foundations for an offshore wind farm in Southern China. Drawing on the experience of designing similar foundations in the North Sea, the paper highlights the challenges faced in the project due to different soil and metocean conditions. The paper identified several areas where further research is needed:

1) Regional experience for CPTU interpretation of soil parameters based on calibration against high quality lab testing is highly valuable but is currently lacking. Engineering geology and geophysical survey should be valued and performed to complement the geotechnical understanding of a site.
2) Silty materials are widely distributed in offshore wind development areas in Southern China. Understanding the static and cyclic properties of these silty materials is essential for the bucket foundation design. Particular attention should be paid to the loose to medium dense silty sands which may exhibit extremely low shear strength under cyclic loading.
3) Understanding of the typhoons. Typhoons are the controlling loading events for caisson foundation design in the region. However, there is limited guidance on the duration and load composition of a typhoon event for geotechnical design.
4) Serviceability limit state design of caisson foundations in soft clays, in particular the assessment of accumulated foundation deformation due to cyclic loading. This requires efforts from the geotechnical profession to further understand the soil mechanics under repeated typhoon loading and potential effects of consolidation between typhoons and under long term average loading. It also requires efforts by the metocean discipline to study the frequency, magnitude and direction of the typhoons using statistical methods. The current design method assumes that all typhoon events approach the turbine in the same direction. This is considered conservative.
5) Installation of suction caissons in layered soils. It is critical to understand the mechanism of suction installation in layered soils and whether seepage flow can be relied on in clay over sand soil profiles. Design methods proposed in literature need to be verified by model testing and field tests.

CRediT authorship contribution statement

Bo Liu: Conceptualization, Methodology, Formal analysis, Investigation, Writing - original draft. **Youhu Zhang:** Conceptualization, Methodology, Formal analysis, Investigation, Writing - original draft. **Zhaorong Ma:** Conceptualization, Investigation, Writing - review & editing. **Knut H. Andersen:** Investigation, Writing - review & editing. **Hans Petter Jostad:** Investigation, Writing - review & editing. **Donghua Liu:** Investigation, Writing - review & editing. **Aiguo Pei:** Project administration, Funding acquisition.

Declaration of competing interest

The authors declare that they have no known competing financial interests or personal relationships that could have appeared to influence the work reported in this paper.

Acknowledgements

The authors are grateful to their respective companies for the permit to publish this paper.

Supplementary materials

Supplementary material associated with this article can be found, in the online version, at doi:10.1016/j.apor.2020.102358.

References

Andersen, K.H., 2015. Cyclic soil parameters for offshore foundation design. In: Meyer (Ed.), The 3rd ISSMGE McClelland Lecture. Frontiers in Offshore Geotechnics III, ISFOG'2015. Taylor & Francis Group, London. ISBN: 978-1-138-02848-7Proc., 5-82. Revised version in http://www.issmge.org/committees/technical-committees/applications/offshore and click on "Additional Information".

Andersen, K.H., Jostad, H.P., Dyvik, R., 2008. Penetration resistance of offshore skirted foundations and anchors in dense sand. J. Geotech. Geoenviron. Eng. 134 (1), 106–116. https://doi.org/10.1061/(ASCE)1090-0241.

Carswel, W., Johansson, J., Løvholt, F., Arwade, S.R., Madshus, C., DeGroot, D.J., Myers, A.T., 2015. Foundation damping and the dynamics of offshore wind turbine monopiles. Renew Energy 80 (2015), 724–736.

Darendeli, M.B., 2001. Development of a new family of normalised modulus reduction curves and material damping curves. PhD thesis. The University of Texas at Austin.

Ding, H., Liu, Y., Zhang, P., Le, C., 2015. Model tests on the bearing capacity of wide-shallow composite bucket foundations for offshore wind turbines in clay. Ocean Eng. 2015 (103), 114–122.

DNVGL (2017). DNVGL-RP-C212 Offshore soil mechanics and geotechnical engineering, Edition August2017.

DNVGL (2018). DNVGL-ST-0126 Support structures for wind turbines, Edition July2018.

Hansteen, O.E. (1984). Equivalent spring stiffnesses for use in dynamic analysis of gravity platforms. NGI Internal report 51400-2, November 30, 1984.

Hardin, B.O., Drnevich, V.P., 1972. Shear modulus and damping in soils: design equations and curves. Journal of Soil Mechanics and Foundation Engineering Div 98 (SM7, June), 667–692 ASCE.

Houlsby, G.T., Byrne, B.W., 2005. Design procedures for installation of suction caissons in sand. Proceedings of the Institution of Civil Engineers, Geotechnical Engineering 158 (GE3), 135–144.

Jamiolkowski, M., Presti, D.C.F.Lo and Manassero, M. (2003). Evaluation of relative density and shear strength of sands from CPT and DMT. ASCE Geotechnical Special

Publication No. 119: 201–238.
Lunne, T., Robertson, P.K., Powell, J.J.M., 1997. Cone Penetration Testing in Geotechnical Practice. Spon Press ISBN 978-0-419-23750-1.
Norwegian Energy Partners (NORWEP) (2019). Annual Global Offshore Wind Market Report 2020-2024. Prepared by BVG Associates August 2019 for NORWEP.
Klinkvort, R.T., Sturm, H., Andersen, K.H., 2019. Penetration model for installation of skirted foundations in layered soils. Journal of Geotechnical and Geoenvironmental Engineering 04019085-1.
Liu, D., Liu, B., Zhang, Y., Ma, Z., Andersen, K.H., Jostad, H.P., Li, L., Zhang, Y., 2020. Long-term settlement of suction caisson foundations supporting offshore wind turbines. In: The 30th (2020) International Ocean and Polar Engineering Conference (ISOPE). Shanghai.
Qi, W.G., Tian, J.K., Zheng, H.Y., Wang, H.Y., Yang, J., He, G.L., Gao, F.P., 2014. Bearing Capacity of the High-Rise Pile Cap Foundation for Offshore Wind Turbines. In: International Conference on Sustainable Development of Critical Infrastructure.
Seed, H.B., Idriss, I.M. (1970). Soil moduli and damping factors for dynamic response analyses, report no. EERC 70.10, Earthquake Engineering Research Center, Berkeley, Cal.
Senders, M., Randolph, M.F., Gaudin, C., 2007. Theory for the installation of suction caissons in sand overlaid by clay. In: Proc., 6th Offshore Site Investigation and Geotechnicics Conference: Confronting New Challenges and Sharing Knowledge. Houston. Offshore Technology Conference, pp. 429–438.
Senders, M., Randolph, M.F., 2009. CPT-based method for the installation of suction caissons in sand. J. Geotech. Geoenviron. Eng. 135 (1), 14–25. https://doi.org/10.1061/(ASCE)1090-0241.
Shonberg, A., Harte, M., Aghakouchak, A., Pachecco, M., Cameron, S.D., Lingaard, M., 2017. Suction caisson jackets for offshore wind turbines: applications from in situ observations. In: Proceedings of the 19th International Conference on Soil Mechanics and Geotechnical Engineering. Soul.
Skau, K.S., Grimstad, G., Page, A.M., Eiksund, G.R., Jostad, H.J., 2018. A macro-element for integrated time domain analyses representing bucket foundations for offshore wind turbines. Mar Struct 59 (2018), 158–178.
Skau, K.S., Jostad, H.P., Eiksund, G., Sturm, H., 2019. Modelling of soil-structure interaction for flexible caissons for offshore wind turbines. Ocean Engineering 171 (2019), 273–285.
Sturm, H., 2017. Design Aspects of Suction Caissons for Offshore Wind Turbine Foundations. In: Proceedings of TC 209 Workshop - Foundation design of offshore wind structures, 19th ICSMGE. Seoul. 20 September 2017.
Sparrevik, P., Strout, J.M., 2015. Novel monitoring solutions solving geotechnical problems and offshore installation challenges. In: Meyer (Ed.), Frontiers in Offshore Geotechnics III. Taylor & Francis Group, London ISBN:978-1-138-02848-7.